Generalized Model of Heat Transfer and Volatiles Evolution Inside Particles for Coal Devolatilization

Binhang Yan, Yan Cheng, Pengcheng Xu, Chenxi Cao, and Yi Cheng
Dept. of Chemical Engineering, Beijing Key Laboratory of Green Chemical Reaction Engineering and Technology, Tsinghua University, Beijing 100084, P.R. China

DOI 10.1002/aic.14484
Published online May 9, 2014 in Wiley Online Library (wileyonlinelibrary.com)

Devolatilization is acknowledged as the first important step in coal conversion techniques. A comprehensive heat transfer and devolatilization model was established, with special consideration of the particle-scale physics and chemistry, to predict the internal heat transport and pyrolysis behavior of particles. The chemical percolation devolatilization model with corrected kinetic parameters and structure parameters was validated with a lot of experimental data and then adopted to describe the devolatilization behaviors under a broader range of temperatures, heating rates, and coal types. The newly achieved understanding of the integrated effect of heating rate and coal type on coal devolatilization could help to provide a preliminary coal rank selection method for industrial processes. In particular, in-depth discussion of the influences of heat conduction, volatiles diffusion, and endothermic heat of devolatilization inside particle indicated the dominant roles of these factors when the intensity of heat transfer was strong or the release of volatiles was rapid.
 AIChE J, 60: 2893–2906, 2014
Keywords: coal, devolatilization, modeling, heat transfer, chemical percolation devolatilization

Introduction

With accelerated depletion of oil and natural gas resources, highly efficient coal conversion techniques to chemicals and alternative fuels are expected to establish their roles in meeting the urgent energy demand in the foreseeable future. At present, most of the coal utilization processes are based on the carbonization, combustion, gasification, pyrolysis to chemicals,[1,2] and so on. As is well-known, coal devolatilization is the first step and also of primary importance in the aforementioned thermal conversion techniques. Thus, the particle heating history and volatiles evolution have significant impacts on the overall reactor performance, especially in the process of coal pyrolysis using thermal plasma. Coal pyrolysis in thermal plasma would open up a direct means to chemicals from coal. However, due to the extreme operating conditions at ultrahigh temperatures and integrated multiple processes in milliseconds, direct measurement inside the reactor can be hardly implemented. Consequently, the detailed devolatilization information of pulverized coals is difficult to be grasped by experiments.[2] Therefore, it is important to establish the fundamental knowledge of coal pyrolysis under a wide range of operating conditions such as heating temperatures, heating rates, coal types, atmospheres, and so on. Because the practical measurements in thermal plasma are not realistic, it is expected to develop theoretic methods to enable reasonable predictions on coal pyrolysis behaviors in such a severe environment (e.g., *ultrahigh* temperature and *ultrafast* heating rate).

The kinetic models proposed to describe coal devolatilization behavior are mainly divided into two types: macromathematical models and chemical models.[3]

The macromathematical models are phenomenological in nature. The simplest model is the single kinetic rate model presented by Badzioch and Hawksley[4] for isothermal processes. The two competing rates (Kobayashi) model[5] is suitable for the nonisothermal cases, in which the devolatilization process is governed by two first-order parallel competing reactions with different activation energies. The distributed activation energy model (DAEM) originally proposed by Pitt[6] assumes that the various organic species presented in coal decompose by an infinite number of independent, parallel and irreversible first-order reactions. All the rate constants share the same preexponential factor but different activation energies varying in a range according to a probability density function (such as Gaussian,[7] Weibull,[8] Gamma,[9,10] or double-Gaussian[11] distributions). Owing to their simplicity, phenomenological models have been proved to be very useful. However, the parameters of each kinetic model depend not only on operating conditions but also on coal types. The kinetic parameters need to be refitted for each coal type as the models do not employ the actual chemical structures.

The representative chemical models include the functional group devolatilization vaporization cross-linking model (FG-DVC),[12,13] the distributed-energy chain statistics (FLASH-CHAIN) model,[14–16] and the chemical percolation devolatilization (CPD).[17–19] Compared to phenomenological models, chemical models describe coal devolatilization in terms of chemical structures and functional groups, making the

Correspondence concerning this article should be addressed to Y. Cheng at yicheng@tsinghua.edu.cn.

predictions more scientific and more applicable over a wide range of coal types. The biggest advantage of the FG-DVC and FLASHCHAIN models is that they adopt a set of *global* kinetic parameters for elementary pyrolysis reactions. However, it is necessary to determine too many coal structure parameters by ^{13}C NMR or FTIR analysis for these two models, thus their applicability is limited drastically. By comparison, the CPD model requires only five coal structure parameters. Besides, the chemical structure parameters can be not only obtained by ^{13}C NMR analysis but also estimated based on ultimate and proximate analyses.[20]

In the above modeling schemes of coal devolatilization processes, the pulverized coal particle is usually assumed isothermal inside. However, due to the inherent heat-transfer and mass-transfer resistances, only the kinetic model may not be adequate to predict the spatiotemporally resolved pyrolysis behavior, especially when the particle size is large in a gasifier/combustor or the particle heating rate is fast in a plasma reactor. Both the large particle size with low heat conductivity and the limited residence time for heat transport would lead to a large temperature gradient/difference within particle. In such cases, special attention must be paid to the heat-transfer resistances *inside* coal particles because the internal heat transfer becomes the rate-controlling factor.

Shuang et al.[21] proved that the heat conduction in coal particles and the diffusion of volatiles were the main resistances impeding the inward heat flow. Fu et al.[22] proposed a devolatilization model coupled with external convective and radiative heat transfer for large coal particles. Adesanya and Pham[23] developed a mathematical model combined with the heat of pyrolysis for large coal particles in a convective heat transfer environment.

However, it is still not clear how the heat-transfer resistances and the devolatilization interact with each other. Therefore, it is essential to establish a comprehensive mathematic model to simultaneously predict both the temperature history and volatiles evolution rate of coal particles. Shuang et al.[21] presented a mechanism model incorporating the heat conduction and diffusion of released volatiles for understanding of the heat transport inside a *single* coal particle under the extreme conditions. In this model, the Kobayashi model was applied as a submodel to depict the coal pyrolysis. Sadhukhan et al.[24] proposed a fully transient and coupled kinetic, heat-transfer model to predict the pyrolysis behavior of a large coal particle, in which the DAEM kinetics was incorporated. A similar model with the DAEM was developed by Liu et al.[25] to numerically analyze coal pyrolysis and heat transfer inside a heated coal particle. The predictions of these models were in very fair agreement with the published experimental data of both pulverized coal and large particles. However, the DAEM and Kobayashi model just provide a chemically reasonable kinetic expression rather than use the actual chemical structures, which severely limits theirs application in describing the devolatilization of various coal types.

In this work, a comprehensive heating and devolatilization mechanism model was established to predict the radial profiles of temperature inside particles and volatiles evolution for various coal types during pyrolysis under different conditions (e.g., a wide range of temperatures and heating rates), considering the following *particle-scale* submodels: (1) CPD model for pyrolysis, (2) heat-transfer model consisting of conductive, convective, and radiative modes for the reacting particle, (3) simplified heat-transfer resistance due to volatiles diffusion inside particle, and (4) endothermic effect of devolatilization. The input parameters of the CPD model were redetermined according to the experimental data of several coals. Then, the particle heating history and volatiles evolution predicted by this model were validated with the experimental findings of the authors and those published in the literature. Furthermore, the integrated effect of heating rate and coal type on the devolatilization performance of a single particle under certain conditions was studied. Finally, the influences of heat conduction, volatiles diffusion, and heat of devolatilization inside particle on particle temperature history and volatiles evolution under different pyrolysis atmosphere were discussed.

Mathematical Model

Model assumptions

To establish a general heat transfer and volatiles evolution model, some basic simplifications and assumptions were made as following:

1. The coal particle is assumed to be a porous sphere, one-dimensional distribution of physical properties with uniform boundary conditions (on the surface).
2. The fragmentation, swelling and shrinkage of coal particles are ignored because the particle volume before and after the pyrolysis are observed experimentally to remain nearly the same.[23]
3. Coal conversion and yield of volatiles are expressed on *Dry Basis* (d, excludes all moisture) or *Dry Ash-Free Basis* (daf, excludes all moisture and ash).
4. A simplified particle-based correction is adopted to consider the impediment of the internal volatiles diffusion on heat transfer.
5. The volatiles and the solid at any local position inside the particle are assumed to be in thermal equilibrium due to the strong interphase heat transfer.
6. The thermal effect of possible ash melting on the temperature of a coal particle is neglected.
7. The temperature and composition of surrounding/heating gas are assumed to be unchangeable during pyrolysis as the mass fraction of coal particles used in the experiments and corresponding simulations is very low.

Heat-transfer model inside a particle

The simplified heat-transfer model within a coal particle was established based on the conduction equation with the consideration of the solid material and the volatiles inside a particle. The energy balance equation inside a particle can be written as

$$\left(\rho_p c_p\right)_{\text{eff}} \frac{\partial T_p(r,t)}{\partial t} = \frac{1}{r^2}\frac{\partial}{\partial r}\left(\lambda_{\text{eff}} r^2 \frac{\partial T_p(r,t)}{\partial r}\right) - \Delta_r H \cdot \gamma_{\text{vol}}(r,t) \tag{1}$$

where

$$\left(\rho_p c_p\right)_{\text{eff}} = \varphi \rho_{\text{vol}} c_{p,\text{vol}} + (1-\varphi)\rho_s c_{p,s} \tag{2}$$

$$\lambda_{\text{eff}} = \varphi \lambda_{\text{vol}} + (1-\varphi)\lambda_s \tag{3}$$

In these equations, $T_p(r,t)$ represents the local temperature at any radial position r and time t; ρ_s and ρ_{vol} are the densities of the solid material and the volatiles within the particle, respectively, $c_{p,s}$ and $c_{p,\text{vol}}$ are the specific heat capacities of the solid material and the volatiles,

respectively, λ_s and λ_{vol} represent the thermal conductivities of the solid material and the volatiles, respectively, λ_{eff} is the effective local thermal conductivity; ϕ is the porosity of particle. $\Delta_r H$ is the heat of devolatilization (J/kg), $\gamma_{vol}(r,t)$ denotes to the rate of devolatilization (kg/m^3 s).

The initial condition is

$$T_p(r,0)=T_{p,init}, \quad \varphi=\varphi_0(0\le r\le R) \tag{4}$$

where, $T_{p,init}$ is the initial temperature of the coal particle, which is typically set to 300 K; ϕ_0 is the initial porosity of particle; R is the particle radius.

The boundary conditions are

$$\begin{cases} 4\pi R^2\lambda_{eff}\left.\dfrac{\partial T_p}{\partial r}\right|_{r=R}=4\pi R^2 h\left(T_g-T_w\right)\theta+\sigma(4\pi R^2)\left(\varepsilon_g T_g^4-\varepsilon_p T_w^4\right) \\ \left.\dfrac{\partial T_p}{\partial r}\right|_{r=0}=0 \end{cases} \tag{5}$$

where, T_w is the temperature at the surface of the coal particle, T_g is local temperature of the surrounding/heating gas; σ is the Stefan–Boltzmann constant, $\sigma = 5.67 \times 10^{-8}$ W/m^2 K^4; ε_p and ε_g are the black-body radiation coefficients of the pulverized coal and the surrounding gas, respectively, h is the gas-particle heat-transfer coefficient, and θ, reported by Spalding,[26] is a factor related to the effect of internal volatiles release on heat transfer.

The gas-particle heat-transfer coefficient is calculated from the Nusselt number Nu, which is estimated as a function of operating conditions and material properties[27]

$$h=\frac{\mathrm{Nu}\,\lambda_g}{d_p} \tag{6}$$

$$\mathrm{Nu}=2\left[1+0.63\mathrm{Re}_g\mathrm{Pr}_g^{0.8}\left(\frac{\mathrm{Pr}_w}{\mathrm{Pr}_g}\right)^{0.42}\left(\frac{\rho_g\mu_g}{\rho_w\mu_w}\right)^{0.52}C^2\right]^{0.5} \tag{7}$$

The parameters in Eq. 7 are defined as follows

$$\mathrm{Re}=\frac{\rho d_p|u_{sl}|}{\mu} \tag{8}$$

$$\mathrm{Pr}=\frac{\mu c_p}{\lambda} \tag{9}$$

$$C=\frac{1-\left(H_w/H_g\right)^{1.14}}{1-\left(H_w/H_g\right)^{2}} \tag{10}$$

where d_p represents the particle diameter; H and μ is the specific enthalpy and viscosity of the surrounding gas, respectively, u_{sl} is the gas-particle slip velocity, which is set to be constant in this work. The subscripts w and g denote that the parameters are calculated with respect to the temperatures of particle surface and surrounding gas, respectively.

The factor θ adopted in this work represents the heat-transfer resistance due to the fast release of volatiles

$$\theta=\frac{B}{e^B-1} \tag{11}$$

$$B=\frac{c_{p,m}}{2\pi d_p\lambda_m}\left(\frac{dm_{vol}}{dt}\right) \tag{12}$$

The subscript m denotes that the parameters are calculated using the temperature of the film between particle surface and bulk fluid, that is

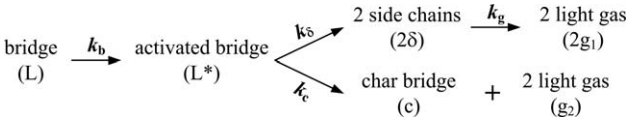

Figure 1. Chemical bridge reaction pathways treated in the CPD model.[28]

$$T_m=\frac{1}{2}\left(T_g+T_w\right) \tag{13}$$

dm_{vol}/dt denotes the formation rate of volatiles from coal (kg/s), that is, the mass change of the particle per unit time. $\theta = 1$ means that there is no volatiles release and no impact on heat transfer to the particle; when devolatilization occurs, $\theta < 1$, it would reduce the gas-particle heat-transfer coefficient.

Devolatilization model

The CPD model,[17–19] which has been demonstrated to predict the yields of light gases and tar as a function of time, temperature, pressure, and coal type,[28,29] is used to describe the devolatilization of coal particles in this work for its wide applicability.

The reaction pathways for the activated bridges, which are adopted to describe the devolatilization behavior of coal in the CPD model, are illustrated in Figure 1.

Lattice bridge, represented by L, forms a reactive/activated bridge intermediate L* by a relatively slow step with rate constant k_b as temperature rises. The activated bridge L* is unstable and reacts quickly in two rapid competitive reactions: one is breaking into two halves of the broken bridges with rate constant k_δ, forming two side chains δ and finally detaching from the infinite lattice as two light gases g_1; the other one is generating a stable char bridge c governed by the rate constant k_c, with the associated release of two light gases g_2. The mass fractions of light gases, tar, and char can be calculated as a function of the ratio of undamaged bridges to broken bridges by the percolation statistics in this model.[17]

A composite rate constant β is defined as the ratio of the rate of side chain formation to the rate of char bridge formation

$$\beta=k_\delta/k_c \tag{14}$$

The competition for the activated bridge L* is governed by the temperature independent ratio β. These coal independent kinetic parameters determined from previously published literature[17–19] are shown in Table 1.

In the CPD model, coal is described with structural parameters obtained experimentally. The five chemical structure parameters are:

- Initial fraction of bridges in the coal lattice, p_0;
- Initial fraction of char bridges, c_0;
- Lattice coordination number, $\psi + 1$;
- Cluster molecular weight, $M_{cluster}$;
- Side chain molecular weight, M_{del}.

In this work, these five parameters are estimated empirically based on ultimate and proximate analyses of various coals.[20]

Physicochemical properties and numerical solution

During the simulation, the physicochemical properties of coals and volatiles are estimated as a function of local

Table 1. Coal Independent Kinetic Parameters for the CPD Model

Parameter	Unit	Description	Literature Value[17–19]	Fitted Value
E_b	cal/mol	Activation energy for bridge breaking	5.540×10^4	$\mathbf{5.762 \times 10^4}$
A_b	s^{-1}	Frequency factor for bridge breaking	2.602×10^{15}	2.602×10^{15}
σ_b	cal/mol	Standard deviation in E_b	1.800×10^3	$\mathbf{4.500 \times 10^3}$
E_g	cal/mol	Activation energy for gas formation	6.90×10^4	$\mathbf{6.946 \times 10^4}$
A_g	s^{-1}	Frequency factor for gas release	3.0×10^{15}	3.0×10^{15}
σ_g	cal/mol	Standard deviation in E_g	8.10×10^3	$\mathbf{1.450 \times 10^4}$
β	–	Ratio of bridge breaking to char bridge formation	0.9	0.9
E_{cross}	cal/mol	Activation energy for cross-linking	6.50×10^4	6.50×10^4
A_{cross}	s^{-1}	Frequency factor for cross-linking	3.0×10^{15}	3.0×10^{15}

The bold characters illustrate values that are changed after fitting.

position and temperature. The physical properties of surrounding gas are given from Boulos et al.[27] as a function of temperature. The volatiles are treated as an ideal mixture of H_2, N_2, CH_4, C_2H_4, C_2H_6, C_3H_8, CO, and CO_2 empirically according to the experimental data. The material properties of the volatiles are calculated by user-defined mixing law based on the properties of each species obtained by kinetic theory.[30] The skeleton density of coal, ρ_s, is assumed to be constant during pyrolysis, while the density of volatiles, ρ_{vol}, is calculated using the ideal gas law. According to the assumption of constant particle volume, the porosity ϕ and the apparent density ρ_p of a coal particle can be obtained through the mass loss of the particle at time t. The thermal conductivity λ_s of the solid in coal is treated as a linearly fitted function based on the experimental data,[31] as

$$\lambda_s = 0.23(1 + 0.0033T_s) \tag{15}$$

The specific heat capacity $c_{p,s}$ is calculated by a method developed by Merrick[32] as a function of T_s. The value of other input parameters, such as the diameter d_p, the initial temperature $T_{p,init}$, the initial porosity ϕ_0 and the skeleton density ρ_s of the coal particle, the atmosphere and the temperature T_g of the surrounding gas, the gas-particle slip velocity u_{sl}, the heat of pyrolysis $\Delta_r H$ and so on, are set according to the specific experiments.

The energy conservation equation (Eq. 1) discretized with second-order discretization in space and first-order discretization in time,[33] is solved by an implicit integral finite volume method. The mass loss equations (i.e., CPD model) are solved by stepwise integration over discrete time steps. The particle is divided into 20–50 shells equally spaced along the radial direction according to the particle size. The time-step size used to integrate the heat and mass transfer equations is automatically adjusted during the different stage of devolatilization reactions to guarantee good convergence for the numerical solutions.

The heat and mass transfer equations are solved in a segregated manner. The two-way coupling between heat transfer and mass transfer is accomplished by alternately calculating the temperature distribution inside particle and the rate of devolatilization until the solutions in both equations converge in a time step. The convergence criterion is set as 10^{-3} for normalized temperature. All the physiochemical properties are updated at each iteration in a time step.

Determination of CPD model parameters

First, the thermal gravimetric analysis (TGA) data of eight different Chinese coals (Coal 1#-8#) were selected to test the general suitability/applicability of the CPD model. The analytical data of these coals are presented in Table 2. The coal-dependent chemical structure parameters of the eight coals for the CPD model are shown in Table 3. All the coals are pulverized, sized to 10–100 μm, dried at 378 K for several hours and then stored in sealed containers.

The TGA pyrolysis conditions are ambient pressure with a N_2 flow of 50 ml/min, from room temperature to 1573 K at a rate of 150 K/min. Small samples (~20 mg coal) are used to ensure uniform heating and to avoid problems of transport phenomena through the sample bed in the sample holder. The variations of the yield of total volatiles (yield of volatiles is defined as the mass loss of coal in TGA, i.e., coal conversion, in this work) with temperature and the differential yield of volatiles with time are shown in Figures 2 and 3, respectively, together with the corresponding predictions by the CPD model.

It can be seen clearly from Figures 2 and 3 that the difference between the TGA data and the model predictions in terms of volatiles amount is obvious. Both the devolatilization rate and the ultimate yield of volatiles for all the eight coals are overestimated by the CPD model. For a particular coal, the ultimate yield of volatiles predicted by the CPD model might be 10–15 wt % higher than that obtained by TGA. This prediction error is a significant amount because the ultimate yield of total volatiles in most of coal pyrolysis processes (even in thermal plasma) is less than 60 wt %. Therefore, to improve the accuracy of model prediction and extend its applicability, the empirical parameters of the CPD model need to be further adjusted or modified.

As shown in Figure 2, the variation trends of the yield of volatiles with temperature for all the eight coal are exactly the same, which serve as an experimental basis for the hypothesis that the kinetic parameters are coal-independent in the CPD model. The kinetic parameters used in the original CPD model, as shown in Table 1, are partly obtained empirically from the relevant literature and partly fitted according to the corresponding experimental data. Although these kinetic parameters allow good agreement between predicted and measured coal devolatilization rates as shown by Fletcher et al.[17–19] for three different coals (i.e., North Dakota lignite, Rosebud subbituminous, and Illinois No. 6 high-volatile bituminous), they are not suitable to describe the devolatilization process of the coals shown in Table 2 due to the overestimation of the devolatilization rate. Therefore, the activation energies for bridge breaking (E_b) and for gas formation (E_g) should be properly increased to reduce the devolatilization rate. Furthermore, the standard deviations in the bridge-breaking activation energy (σ_b) and in the gas formation activation energy (σ_g) also need to be increased to ensure that the formation of light gas g_1 from the breakdown of side chains δ could occur at relatively low temperatures. Based on the TGA data of the eight different coals, the coal-independent kinetic parameters (E_b, E_g, σ_b and σ_g) are refitted and also presented in Table 1.

Table 2. Chemical Analyses of Coals

Coals			Proximate Analysis, wt %				Ultimate Analysis, wt %				
Origin	Name	Number	M_{ad}	A_d	V_d	FC_d	C_{daf}	H_{daf}	O_{daf}	N_{daf}	S_{daf}
Xinjiang	Heishan coal	1#	3.58	17.76	32.86	49.38	76.77	4.89	17.49	1.55	0.58
Xinjiang	Xinjiang coal	2#	3.66	15.18	34.61	50.21	76.49	4.85	17.20	1.54	0.53
Xinjiang	Miquan coal	3#	3.60	12.20	37.92	49.88	78.28	5.21	14.09	1.69	0.74
Inner Mongolia	Shangwan coal	4#	4.42	4.88	34.35	60.77	77.33	4.44	16.41	1.18	0.29
Inner Mongolia	Qihua coal	5#	4.11	12.51	31.74	55.74	77.82	4.29	17.28	1.18	0.45
Ningxia	Lingxin coal	6#	9.65	7.56	28.52	63.93	77.44	3.63	17.85	1.14	0.19
Ningxia	Yangchangwan coal	7#	8.36	10.53	28.18	61.29	76.00	3.60	20.32	1.02	0.40
Ningxia	Qipanjing coal	8#	1.20	12.84	25.19	61.97	83.76	4.72	8.77	1.56	0.89
Ningxia	Qingshuiying coal	9#	14.46	5.84	29.46	64.70	90.69	4.59	2.50	1.24	0.98
Ref. 11	Sulcis coal	10#	5.10	15.40	42.70	41.90	74.70	5.50	10.20	1.30	8.30
Ref. 11	Russian coal	11#	4.10	13.30	8.90	77.80	86.60	4.10	8.20	0.70	0.40
Ref. 34	Yallourn	12#	15.00	1.18	53.29	45.53	65.40	4.90	28.80	0.60	0.30
Ref. 34	Rhein Braun	13#	20.30	2.89	54.83	42.28	65.80	5.50	27.60	0.80	0.30
Ref. 34	Morwell	14#	19.60	1.99	51.49	46.52	67.40	5.00	26.80	0.50	0.30
Ref. 34	Velva	15#	15.80	8.79	47.74	43.47	69.10	4.80	23.90	1.40	0.60
Ref. 34	Soyakoishi	16#	17.70	9.96	41.80	48.24	70.20	5.20	22.40	1.80	0.20
Ref. 34	South Beulah	17#	18.10	13.68	38.58	47.74	71.80	4.70	19.20	1.40	2.90
Ref. 34	Colowyo	18#	13.20	6.34	36.29	57.37	74.00	5.00	18.60	1.90	0.40
Ref. 34	Taiheiyo	19#	4.40	12.24	49.16	38.60	76.00	6.50	16.00	1.20	0.30
Ref. 34	Millmerran	20#	6.60	16.38	45.82	37.79	74.90	6.60	15.40	0.50	0.60
Ref. 34	Wandoan	21#	10.40	8.26	45.65	46.09	78.50	5.80	14.40	0.90	0.40
Ref. 34	Hunter Valley	22#	4.40	9.41	33.68	56.90	80.30	5.00	12.20	2.00	0.40
Ref. 34	Liddell	23#	3.70	8.00	34.58	57.42	83.50	5.40	8.40	2.10	0.60
Ref. 34	Newvale	24#	3.30	14.37	29.27	56.36	84.20	5.00	8.90	1.40	0.50
Ref. 34	Yubari Shinko	25#	1.10	5.16	38.42	56.42	86.90	5.60	5.20	1.90	0.30
Ref. 34	Vicary Creek	26#	2.20	12.37	21.68	65.95	87.80	4.70	5.00	2.10	0.40
Ref. 34	Keystone	27#	1.60	5.18	15.96	79.07	89.40	4.40	3.20	2.20	0.80
Ref. 34	Hongay	28#	1.60	4.47	7.32	88.21	93.80	3.00	1.40	1.30	0.50
Ref. 35	Pittsburgh No.8	29#	2.50	13.70	33.40	52.90	84.20	5.54	7.56	1.65	1.01

Conversely, much attention should be paid to the chemical structure parameters to enhance the predictive accuracy for the ultimate yield of volatiles. In the CPD model, the initial coal mass is divided into light gases, tar, metaplast (which are referred to the finite fragments that remain in the condensed phase), and char. A vapor–liquid equilibrium and a

Table 3. Chemical Structure Parameters of Coals for CPD Model

Coals			Chemical Structure Parameter					
Origin	Name	Number	p_0	c_0	$\psi+1$	$M_{cluster}$	M_{del}	M_{sub}
Xinjiang	Heishan coal	1#	0.607	0.070	5.09	318.00	37.10	15.235
Xinjiang	Xinjiang coal	2#	0.601	0.066	5.11	320.96	37.55	14.951
Xinjiang	Miquan coal	3#	0.538	0.022	5.08	343.11	36.83	15.643
Inner Mongolia	Shangwan coal	4#	0.643	0.055	5.26	310.81	35.24	17.582
Inner Mongolia	Qihua coal	5#	0.669	0.067	5.28	298.23	34.00	16.408
Ningxia	Lingxin coal	6#	0.721	0.075	5.59	332.73	33.11	17.123
Ningxia	Yangchangwan coal	7#	0.742	0.109	5.61	335.46	34.17	14.836
Ningxia	Qipanjing coal	8#	0.635	0.000	5.00	294.38	26.93	16.625
Ningxia	Qingshuiying coal	9#	0.666	0.360	4.16	234.17	18.98	−3.011
Ref. 11	Sulcis coal	10#	0.410	0.000	5.30	435.85	42.77	12.087
Ref. 11	Russian coal	11#	0.834	0.119	4.65	251.97	17.78	14.734
Ref. 34	Yallourn	12#	0.675	0.150	4.13	339.20	49.99	6.570
Ref. 34	Rhein Braun	13#	0.597	0.150	3.98	387.32	52.39	−0.891
Ref. 34	Morwell	14#	0.645	0.150	4.39	342.33	48.06	7.945
Ref. 34	Velva	15#	0.623	0.150	4.62	334.68	46.56	9.376
Ref. 34	Soyakoishi	16#	0.578	0.139	4.61	369.01	47.31	12.788
Ref. 34	South Beulah	17#	0.587	0.094	4.93	348.75	44.55	16.555
Ref. 34	Colowyo	18#	0.590	0.085	4.98	350.49	41.53	18.800
Ref. 34	Taiheiyo	19#	0.359	0.049	4.87	528.32	45.64	−6.370
Ref. 34	Millmerran	20#	0.323	0.041	4.87	570.86	48.49	−8.194
Ref. 34	Wandoan	21#	0.467	0.027	4.94	394.68	38.81	7.916
Ref. 34	Hunter Valley	22#	0.574	0.000	5.10	322.53	33.23	18.296
Ref. 34	Liddell	23#	0.528	0.000	4.91	341.81	30.44	15.390
Ref. 34	Newvale	24#	0.594	0.000	4.84	296.73	28.21	17.447
Ref. 34	Yubari Shinko	25#	0.508	0.154	4.57	337.43	27.15	2.810
Ref. 34	Vicary Creek	26#	0.674	0.260	4.56	265.35	21.15	6.872
Ref. 34	Keystone	27#	0.755	0.360	4.44	250.24	16.09	3.780
Ref. 34	Hongay	28#	0.918	0.360	3.95	284.29	9.70	3.364
Ref. 35	Pittsburgh No.8	29#	0.508	0.000	4.85	353.08	30.14	4.837

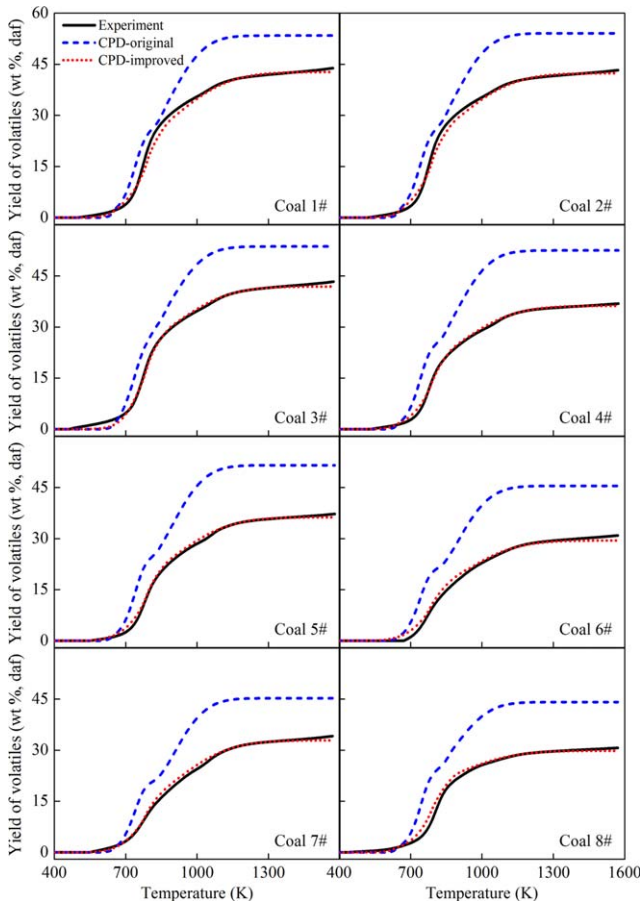

Figure 2. Comparison among the experimental yields of volatiles, the original CPD predictions and the improved CPD predictions as a function of temperature for Coal 1#-8# (N_2 atmosphere, heating rate 150 K/min, ultimate temperature 1573 K).

[Color figure can be viewed in the online issue, which is available at wileyonlinelibrary.com.]

simple cross-linking mechanism are adopted to determine the amount of metaplast that is vaporized as tar and reattached to the infinite char matrix, respectively. The yields of tar and light gases predicted by the CPD model are directly related to the molecular weight of the cluster ($M_{cluster}$) and the molecular weight of the side chain (M_{del}), which are determined by the NMR measurements. However, some functional groups (such as tightly bound a-methyl groups), which are counted as side chains in the NMR measurements, should be considered as part of the aromatic cluster in the CPD model because they are not released during devolatilization.[19] To make sure that the model predictions are in a good agreement with experimental values, the side chain molecular weight (M_{del}) used in the CPD model is reduced empirically by 7 for all coals. From our point of view, the correction of side chain molecular weight (M_{sub}, which represents the fraction of tightly bound side chains) is dependent on coal type and should be served as the *sixth* structure parameter. M_{sub} can be fitted according to the proximate analysis or pyrolysis experimental data for an arbitrary coal type. Therefore, M_{sub} is a coal-dependent parameter rather than assumed as a constant in the original CPD model, as shown in Table 3.

Base on the refitted coal-independent kinetic parameters (shown in Table 1) and the coal-dependent chemical structure parameters (shown in Table 3), the volatiles evolution and the variations of the differential yield of volatiles with time predicted by the improved CPD model are plotted on Figures 2 and 3, respectively. As shown in Figures 2 and 3, the predictions agree well with the experimental data for all the eight coals, indicating that the predictive accuracy of the improved CPD model is markedly raised. Therefore, this model is applicable to the description and the analysis of devolatilization processes of various coal types under different conditions.

Results and Discussion

Model validation

Three sets of test cases were used to validate the reliability and applicability of this comprehensive mechanism model. The first test case was a series of slow pyrolysis experiments in furnace using dried coal samples (Coal 1#-9#, ~50 μm) with an Ar flow of 20 ml/min. The heating rate was 40 K/min and the ultimate temperature was 1173 K.

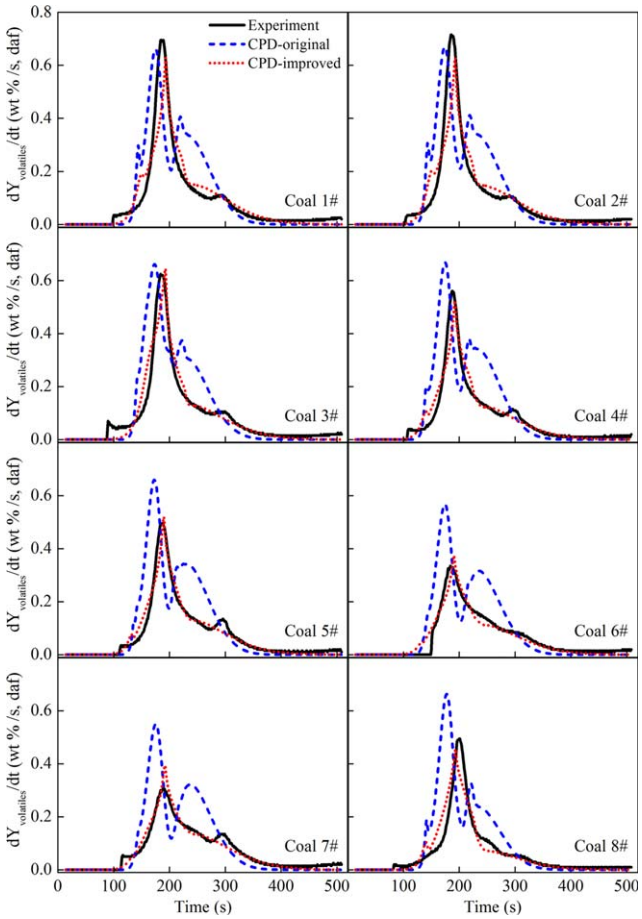

Figure 3. Comparison among the experimental differential yields of volatiles, the original CPD predictions and the improved CPD predictions as a function of time for Coal 1#-8# (N_2 atmosphere, heating rate 150 K/min, ultimate temperature 1573 K).

[Color figure can be viewed in the online issue, which is available at wileyonlinelibrary.com.]

Table 4. Predicted and Experimental Yields of Volatiles and Light Gases for 28 Coals

Coals			Yield of Volatiles, wt %, daf		Yield of Light Gases, wt %, daf	
Origin	Name	Number	Experimental	Improved CPD	Experimental	Improved CPD
Xinjiang	Heishan coal	1#	40.8	41.0	34.2	29.7
Xinjiang	Xinjiang coal	2#	41.7	40.7	22.0	29.2
Xinjiang	Miquan coal	3#	41.4	40.5	25.0	25.0
Inner Mongolia	Shangwan coal	4#	35.3	34.7	22.2	24.8
Inner Mongolia	Qihua coal	5#	36.8	34.9	23.4	25.9
Ningxia	Lingxin coal	6#	32.0	28.4	21.8	23.0
Ningxia	Yangchangwan coal	7#	30.5	31.6	24.1	27.4
Ningxia	Qipanjing coal	8#	27.8	28.5	15.9	14.4
Ningxia	Qingshuiying coal	9#	30.1	33.0	15.2	25.9
Ref. 11	Sulcis coal	10#	44.2	41.3	–	23.4
Ref. 11	Russian coal	11#	10.2	10.5	–	4.6
Ref. 34	Yallourn	12#	51.0	51.5	31.1	37.7
Ref. 34	Rhein Braun	13#	52.5	54.8	30.4	37.6
Ref. 34	Morwell	14#	55.5	50.1	29.9	36.8
Ref. 34	Velva	15#	48.5	49.8	30.6	37.0
Ref. 34	Soyakoishi	16#	49.0	45.1	28.1	30.2
Ref. 34	South Beulah	17#	47.0	43.4	30.2	28.4
Ref. 34	Colowyo	18#	41.5	38.2	22.2	23.1
Ref. 34	Taiheiyo	19#	53.0	55.3	23.4	32.2
Ref. 34	Millmerran	20#	51.5	55.9	21.7	32.5
Ref. 34	Wandoan	21#	52.0	49.6	24.1	26.1
Ref. 34	Hunter Valley	22#	38.0	37.9	16.1	16.7
Ref. 34	Liddell	23#	39.5	39.5	17.3	14.5
Ref. 34	Newvale	24#	35.5	35.4	16.1	12.1
Ref. 34	Yubari Shinko	25#	38.0	40.9	16.0	21.1
Ref. 34	Vicary Creek	26#	24.5	24.0	12.8	16.0
Ref. 34	Keystone	27#	17.0	16.6	8.9	13.1
Ref. 34	Hongay	28#	6.0	7.3	3.4	5.1

The second experimental tests were performed with a thermogravimetric analyzer.[11] The tests were carried out in a N_2 inert atmosphere with a heating rate of 100 K/min. The Sulcis sample (Coal 10#, ~65 μm) was heated to 1223 K, while the Russian sample (Coal 11#, ~65 μm) was heated to a higher temperature, 1350 K. The samples were maintained at the maximum temperature for 10 min. The last set of test cases reported by Xu and Tomita[34] was flash-pyrolysis experiment in a Curie-point pyrolyzer at 1037 K in Ar atmosphere, using 17 coals (Coal 12#-28#, ~70 μm) ranging from lignite to anthracite. The coal samples were heated at a rate of 3000 K/s to the ultimate temperature of 1037 K and with a residence time of 4 s at that temperature. The corresponding proximate analysis data, ultimate analysis data and six estimated structural parameters of these coals are listed in Tables 2 and 3, respectively. Table 4 lists the measured and predicted yields of total volatiles and light gases for the 28 coals. Figure 4 shows the predicted ultimate yields of volatiles and light gases and the corresponding experimental data vs. volatile matter content (wt %, daf) in the parent coal. It can be seen from Figure 4 that the predictions fit in well with the values of the corresponding experimental yields of volatiles and the trend of the yield of light gases for most of the coals tested. The average relative errors between the measured data and the predicted values are 5.1% for the yield of volatiles and 21.8% for the yield of light gases. This indicates that the improved CPD model is applicable to the description of coal devolatilization processes with different coal types, although it is not accurate enough yet to predict the yield of light gases.

Furthermore, this model can be also used to predict the coal devolatilization behaviors at high temperatures with a wide range of heating rates. Take the cases of Heishan bituminous coal (Coal 1#, ~50 μm) and Pittsburgh No.8 bituminous coal (Coal 29#, ~70 μm), for example. The Heishan samples were investigated in a drop tube reactor[36] at an ultimate temperature of 1473 K with Ar as the carrier gas. The heating rate was set to 0.1 K/s in the slow pyrolysis experiment. Although in the fast pyrolysis process, the heating rate was estimated at about 6×10^3 K/s. The effect of heating rate (from 10 K/s to 2×10^4 K/s) on the yield of volatiles of Pittsburgh No.8 coal reported by Griffin et al.[35] was measured in an electrical screen heater at 1073 K with an atmosphere of He (and then maintained at the maximum temperature for 15 s). The predicted yields of volatiles as a function of heating rate are plotted in Figure 5, together with the corresponding experimental data. As shown in Figure 5, the predicted yields of volatiles agree quite well with the experimental data in a wide range of heating rates. Although the model prediction is not accurate enough for some unusual coals, this comprehensive model is proved to be well-suited to provide a creditable prediction of devolatilization behaviors for various coal types under a broader range of temperatures and heating rates.

Effect of particle heating rate

The typical effect of heating rate on the devolatilization of Sulcis subbituminous coal (Coal 10#) was studied, as shown in Figure 6. In these numerical experiments, coal particles were heated from 300 to 1800 K at different preset rates (from 10^{-1} to 10^6 K/s) with zero hold time at the ultimate temperature before quenching. As it takes time for the breaking of the labile bonds between the aromatic clusters and the formation of new chemical bonds, the increase of heating rate will increase the temperature at which the devolatilization reactions occur. As illustrated in Figure 6, the volatiles release curve shifts to higher temperature section as heating rate increases. The yield of total volatiles significantly

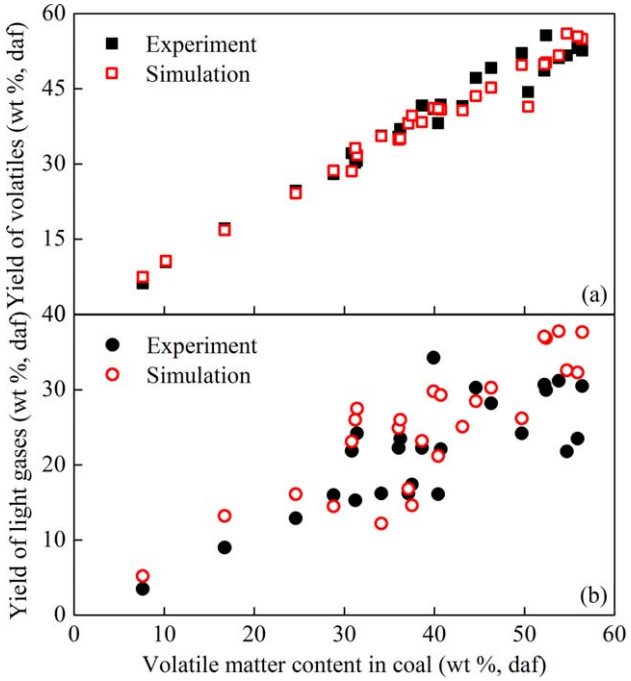

Figure 4. Comparison between the experimental data and model predictions as a function of volatile matter content in coal: (a) yield of volatiles, (b) yield of light gases (Coal 1#-9#: Ar atmosphere, heating rate 40 K/min, ultimate temperature 1173 K; Coal 10#: N_2 atmosphere, heating rate 100 K/min, ultimate temperature 1223 K; Coal 11#: N_2 atmosphere, heating rate 100 K/min, ultimate temperature 1350 K; Coal 12#-28#: Ar atmosphere, heating rate 3000 K/s, ultimate temperature 1037 K).

[Color figure can be viewed in the online issue, which is available at wileyonlinelibrary.com.]

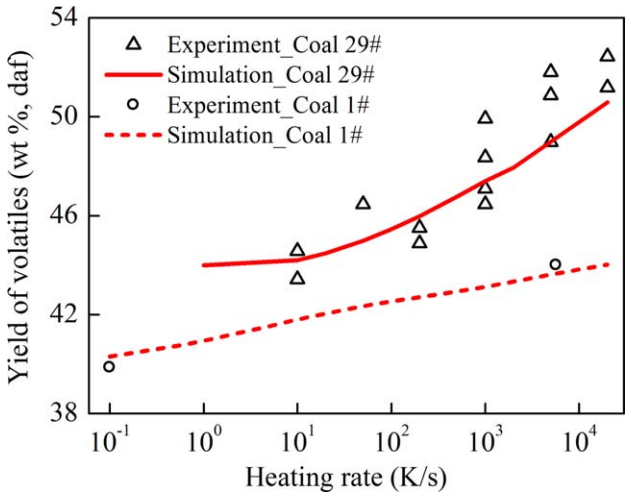

Figure 5. Comparison between the experimental yields of volatiles and model predictions as a function of heating rate (Coal 1#: Ar atmosphere, ultimate temperature 1473 K; Coal 29#: He atmosphere, ultimate temperature 1073 K).

[Color figure can be viewed in the online issue, which is available at wileyonlinelibrary.com.]

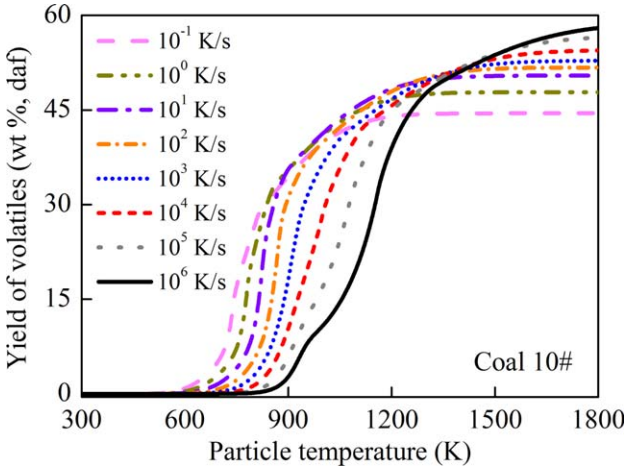

Figure 6. Variation of predicted yield of volatiles with particle temperature at different heating rates (Coal 10#, initial particle temperature 300 K, surrounding temperature 1800 K).

[Color figure can be viewed in the online issue, which is available at wileyonlinelibrary.com.]

increases from 44.5 to 58 wt % when the heating rate increases from 10^{-1} to 10^{6} K/s. The simulation results are in agreement with the previous work reported by Fletcher.[18]

Figure 7 shows the yields of volatiles for Sulcis subbituminous coal at eight different heating rates when the ultimate temperature is varied from 800 to 1800 K with zero hold time before quenching. The lines with symbols represent the yields of volatiles when the coal samples reach the same ultimate temperature within different heating time (which is corresponded to different heating rate). When the yield of total volatiles is taken as the representative of devolatilization performance, the heating rate is not the faster the better because the devolatilization process is not completely finished under certain conditions (e.g., the final temperature below 1400 K). When the ultimate temperature is comparatively high (such as 1800 K), the devolatilization time of the particle (which is defined as the residence time required for finishing the devolatilization process) is greater than or approximately equal to the heating time (i.e., the residence time). In these cases, the devolatilization reactions are carried out in a complete way. Consequently, the yield of total volatiles shows the tendency of increasing with heating rate. When the ultimate temperature is low (such as 1000 K), the devolatilization time is much less than the heating time, and the faster the heating rate is, the greater the time-lag is. Therefore, to obtain an excellent reactor performance, it is very important to match the residence time with the devolatilization time in a practical coal thermal conversion process.

When the residence time of coal particle at high temperature zone is long enough, the yield of volatiles would increase with the increase of heating rate, as shown in Figure 6. As discussed in the previous work,[18] the predicted change in the yield of volatiles with heating rate is dominated by the temperature independent ratio β, which governs the competitive consumption of the activated bridge L^{*}. In addition, the increased heating rate would lead to a more rapid release of volatiles and accordingly result in a pressure build-up within the pore structure.[36] The yield of volatiles might increase due to this pressure build-up since it could rapidly expel more fragments from coal particle and reduce the

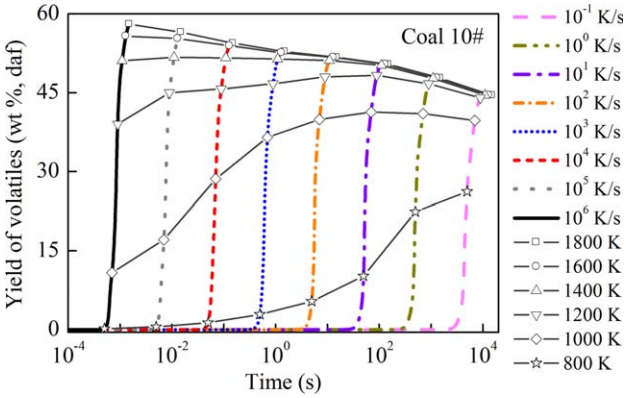

Figure 7. Variation of predicted yield of volatiles with time at different heating rates (Coal 10#, initial particle temperature 300 K, surrounding temperature 1800 K).

[Color figure can be viewed in the online issue, which is available at wileyonlinelibrary.com.]

cross-linking reaction from metaplast to char. Therefore, the change in the yield of volatiles depends on the detailed chemical structure of coal (i.e., coal type).

To explore the influence of coal type on the change of the yield of volatiles with increasing heating rate from 10^{-1} to 10^6 K/s, a number of numerical experiments were carried out. In these calculations, the coal samples (Coal 1#-29#) were heated from 300 to 1800 K at two designated rates (10^{-1} and 10^6 K/s) with enough hold time at 1800 K before quenching. The simulation results are shown in Table 5. For increasing heating rate from 10^{-1} to 10^6 K/s, the change of the yield of volatiles of different coals varies widely, from as little as 0.15 wt % (Coal 27#) to as much as 16.4 wt % (Coal 20#). As shown in Table 5, although there seems to be no definitive relationship between the change of the yield of volatiles with the change of heating rate and coal type, some guidelines can be made such as that which coals would show a good devolatilization performance as heating rate rises.

For the process of coal pyrolysis in thermal plasma mentioned in the Introduction section, because the rector performance is mainly dominated by the yield of total volatiles[2] (coal conversion in this process is usually less than 60 wt %), the increase of the yield of volatiles at high heating rates (such as 10^6 K/s) by 10 wt % or even much of dry ash-free (daf) coal (such as Coal 10#, 19#, 20#, 23#, and 24#) is a significant amount. Therefore, the simulations can help to provide a quick method of preliminary coal rank selection for industrial plasma pyrolysis process.

Effect of inherent heat-transfer resistances

As mentioned above, both the inherent resistances of heat conduction and diffusion of released volatiles will affect coal devolatilization performance, especially when the particle size is large or the particle heating rate is fast. To investigate the specific influences of the two resistances under various conditions (e.g., H_2 atmosphere and/or Ar atmosphere), and to judge under which conditions the inherent resistances have to be considered or can be ignored, four different cases of numerical experiments on the devolatilization of Heishan bituminous coal (Coal 1#) were performed:

Table 5. Predicted Yields of Volatiles at Two Designated Rates (10^{-1} and 10^6 K/s) for 29 Coals

Coals			Yield of Volatiles, wt %, daf	
Origin	Name	Number	10^{-1} K/s	10^6 K/s
Xinjiang	Heishan coal	1#	40.299	44.845
Xinjiang	Xinjiang coal	2#	41.417	46.053
Xinjiang	Miquan coal	3#	41.097	49.250
Inner Mongolia	Shangwan coal	4#	35.253	38.978
Inner Mongolia	Qihua coal	5#	35.496	37.962
Ningxia	Lingxin coal	6#	29.118	30.354
Ningxia	Yangchangwan coal	7#	32.591	33.075
Ningxia	Qipanjing coal	8#	28.244	36.596
Ningxia	Qingshuiying coal	9#	33.970	34.751
Ref. 11	Sulcis coal	10#	44.477	58.725
Ref. 11	Russian coal	11#	10.244	11.511
Ref. 34	Yallourn	12#	53.617	57.120
Ref. 34	Rhein Braun	13#	56.171	61.589
Ref. 34	Morwell	14#	52.244	55.475
Ref. 34	Velva	15#	52.128	54.952
Ref. 34	Soyakoishi	16#	45.794	50.547
Ref. 34	South Beulah	17#	43.791	48.444
Ref. 34	Colowyo	18#	37.641	42.983
Ref. 34	Taiheiyo	19#	49.159	64.142
Ref. 34	Millmerran	20#	48.919	65.361
Ref. 34	Wandoan	21#	47.163	57.344
Ref. 34	Hunter Valley	22#	34.692	43.681
Ref. 34	Liddell	23#	35.272	46.865
Ref. 34	Newvale	24#	30.489	41.419
Ref. 34	Yubari Shinko	25#	38.955	46.942
Ref. 34	Vicary Creek	26#	24.743	26.193
Ref. 34	Keystone	27#	17.925	18.075
Ref. 34	Hongay	28#	7.664	7.933
Ref. 35	Pittsburgh No.8	29#	46.271	56.079

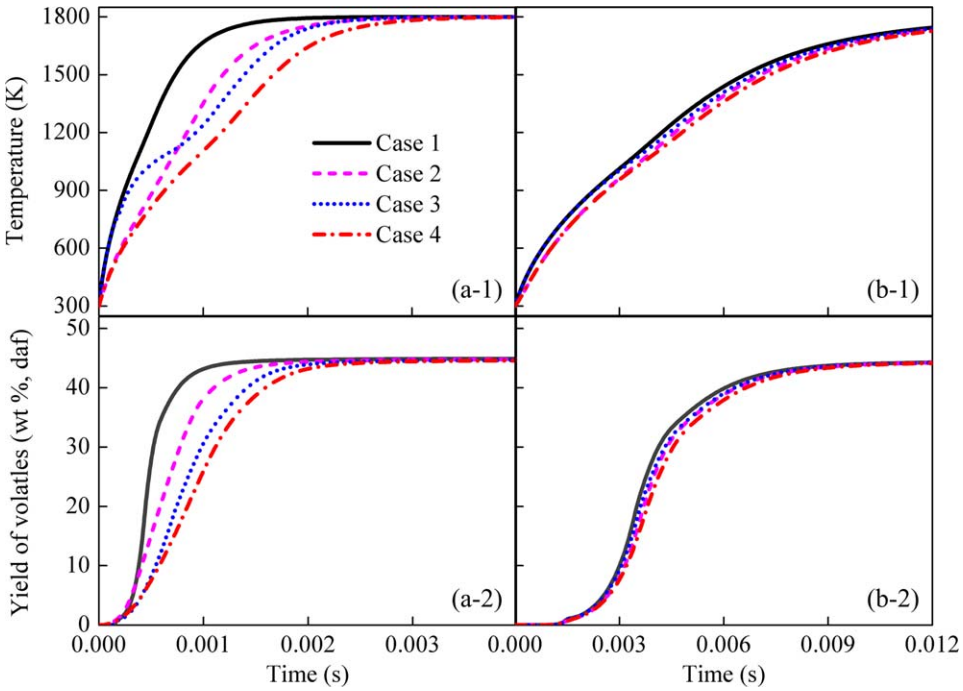

Figure 8. Variations of (1) particle average temperature and (2) yield of volatiles with time in (a) H_2 atmosphere and (b) Ar atmosphere of different Cases (Coal 1#, initial particle temperature 300 K, particle diameter 50 μm, surrounding temperature 1800 K).

[Color figure can be viewed in the online issue, which is available at wileyonlinelibrary.com.]

1. Case 1: neither of the two resistances is considered with the assumptions of $\theta = 1$ and $\lambda_s = 1 \times 10^{10}$ W/m K;
2. Case 2: only the inherent resistance due to heat conduction is considered with the assumption of $\theta = 1$;
3. Case 3: only the inherent resistance due to volatiles release is considered with the assumption of $\lambda_s = 1 \times 10^{10}$ W/m K;
4. Case 4: both of the two resistances are considered.

In these simulations, the radiant heat transfer and the endothermic effect of devolatilization were ignored. The temperature of the surrounding gas was fixed at 1800 K, the gas-particle slip velocity u_{sl} was set to 20 m/s, the initial temperature of the coal particle was 300 K, and the diameter of the particle was 50 μm.

The effects of the inherent heat-transfer resistances on the average temperature and devolatilization performance of the particle under the atmosphere of H_2 and Ar are plotted in Figure 8a, b, respectively. It is clearly seen that the inherent resistance due to heat conduction affects the particle temperature throughout the course of heating while the resistance due to volatiles diffusion affects the particle temperature once the devolatilization reactions occur. Both inherent resistances would impede the thermal energy transportation from heating gas to the particle, leading to a weakened heating-up rate, that is, a longer heating-up and devolatilization time. However, the influence of the inherent resistances on particle heating history and volatiles evolution depends strongly on the pyrolysis condition. When the surrounding gas is H_2, as shown in Figure 8a, significant difference exists between the devolatilization processes of Case 1 and Case 4: the biggest temperature difference and volatiles yield difference are as high as 568.3 K (time = 0.94 ms) and 24.4 wt % (time = 0.64 ms), respectively, moreover, the difference of devolatilization time is distinct as well (1.54 ms for Case 1 and 2.60 ms for Case 4). While in Ar atmosphere, the biggest temperature difference and volatiles yield difference are only 63.6 K (time = 7.5 ms) and 5.9 wt % (time = 3.7 ms), respectively, and the devolatilization time of Case 1 (10.1 ms) is almost the same as that of Case 4 (10.8 ms).

The aforementioned fact, that is, the strong dependence of devolatilization performance on the surrounding gas, can be attributed to the different thermodynamic and transport properties of the gas. Because the specific heat capacity and the thermal conductivity of H_2 are much higher than those of Ar at the temperature of 1800 K, the gas-particle heat-transfer coefficient in H_2 atmosphere ($\sim 3.3 \times 10^4$ W/m^2 K) is almost an order of magnitude higher than that in Ar atmosphere ($\sim 3.5 \times 10^3$ W/m^2 K). Generally, the temperature gradient inside particle is proportional to the gas-particle heat-transfer coefficient. This explains why the biggest temperature difference between Case 1 and Case 4 in H_2 atmosphere is almost 10-times higher than that in Ar atmosphere. Therefore, whether the inherent heat-transfer resistances should be considered or not is dominated by *the intensity of heat transfer*, which is mainly determined by the particle size, surrounding temperature and atmosphere.

Figure 9 shows the variations of the maximum temperature difference and volatiles yield difference inside particle as a function of residence time under the atmosphere of H_2 and Ar. It can be obviously seen that the temperature gradient inside particle is much higher when the particle pyrolyses in H_2 atmosphere than that in Ar atmosphere: the peak values of the maximum temperature difference and volatiles yield difference inside particle are as high as 739 K (time = 0.29 ms) and 36.1 wt % (time = 0.71 ms), respectively, in the former situation; while are only 203 K (time = 0.48 ms) and 11.6 wt % (time = 3.63 ms), respectively, in the latter

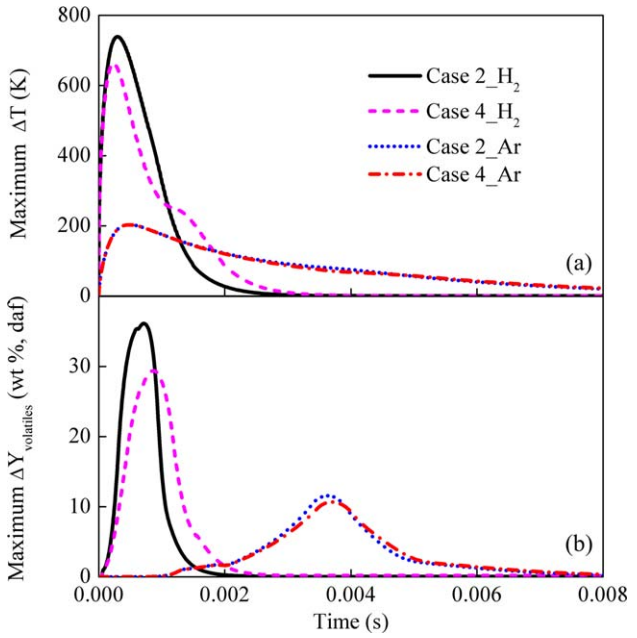

Figure 9. Variations of (a) maximum temperature difference and (b) maximum volatiles yield difference inside particle with time in H_2 atmosphere and Ar atmosphere of Case 2 and Case 4 (Coal 1#, initial particle temperature 300 K, particle diameter 50 μm, surrounding temperature 1800 K).

[Color figure can be viewed in the online issue, which is available at wileyonlinelibrary.com.]

case. This is in conformity with the aforementioned conclusion that *the intensity of heat transfer* in H_2 atmosphere is much higher than that in Ar atmosphere. That is to say, the maximum gradient of temperature will increase with the enhancement of the intensity of heat transfer. Correspondingly, the temperature gradient inside particle would disappear more rapidly when the intensity of heat transfer is stronger. To get a uniform temperature distribution inside particle, it takes only 2.5 ms when the particle pyrolyses in H_2 atmosphere but more than 15 ms in Ar atmosphere, as shown in Figure 9. In addition, the temperature gradient inside particle rapidly increases up to the peak value within 0.5 ms when the particle is mixed well with the high temperature gas no matter under the atmosphere of H_2 or Ar.

When a particle pyrolyses in Ar atmosphere with the diameter no more than 50 μm and the temperature lower than 1800 K, the heat transfer is relatively moderate and thereby the release of volatiles is slow. Hence, the inhibition of the volatiles diffusion on the heat transfer from surrounding gas to particle can be ignored. Thus, there is almost no difference that the inherent resistance due to volatiles release is considered or not, as shown in Figures 8b and 9. But, when a particle pyrolyses in H_2 atmosphere at 1800 K, both the inherent resistances have to be considered even if the particle has a diameter as small as 10 μm.

However, when the attention is only focused on the final results (such as the ultimate particle temperature and yield of volatiles) rather than the course/process of reactions, the inherent resistances can also be ignored in some cases that the residence time of the particle in high temperature zone is long enough to completely finish the devolatilization reactions. Therefore, a residence-time criterion which comprehensively takes into account the interaction among particle size, surrounding temperature and atmosphere could be defined to judge whether the inherent resistances can be ignored in those cases. In this work, the critical time (which is slightly less than the devolatilization time) is defined as the residence time at which the relative error between the predicted yields of volatiles with and without the consideration of the inherent resistances is less than 5%. The critical time is meant to change when the particle size, the surrounding temperature or the atmosphere changes. Figure 10 shows the relationships among the critical time, the particle diameter and the surrounding temperature in H_2 atmosphere when the inherent heat-transfer resistances can be ignored. It can be concluded that a higher surrounding temperature as well as a longer particle residence time in high temperature zone would lead to a larger particle diameter that the inherent resistances can be ignored.

However, it should be noted that the inherent resistances must be considered seriously when the particle residence time in a practical reactor is less than the critical time estimated under the same condition. In such situations, the radial profiles of the temperature and particle mass loss (i.e., yield of volatiles) inside particle at any time can be accurately predicted by the model proposed in this work. The model-predicted temperature profiles and particle mass loss profiles during devolatilization of Case 4 in H_2 atmosphere are plotted in Figure 11. Figure 11 shows a fast release of volatiles because of the rapid heating of the particle. It is interesting to note that both the radial temperature and mass loss profiles are nearly flat after the critical time (i.e., 1.85 ms, at which the devolatilization reactions is almost complete). This suggests that the effect of heat conduction becomes insignificant when the particle residence time is larger than 1.85 ms, which is in agreement with the earlier results.

Effect of heat of devolatilization

To clarify the effect of reaction heat of devolatilization, the devolatilization behaviors of Heishan bituminous coal

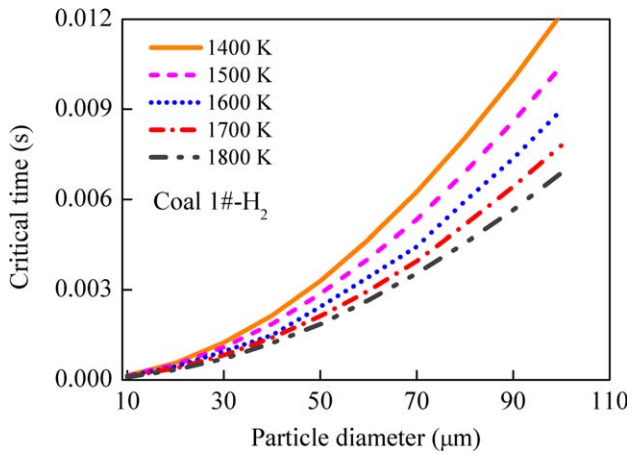

Figure 10. Predicted relationship among the critical time, the particle diameter and the surrounding temperature in H_2 atmosphere when the inherent resistances can be ignored (Coal 1#, initial particle temperature 300 K, particle diameter 50 μm, surrounding temperature 1800 K).

[Color figure can be viewed in the online issue, which is available at wileyonlinelibrary.com.]

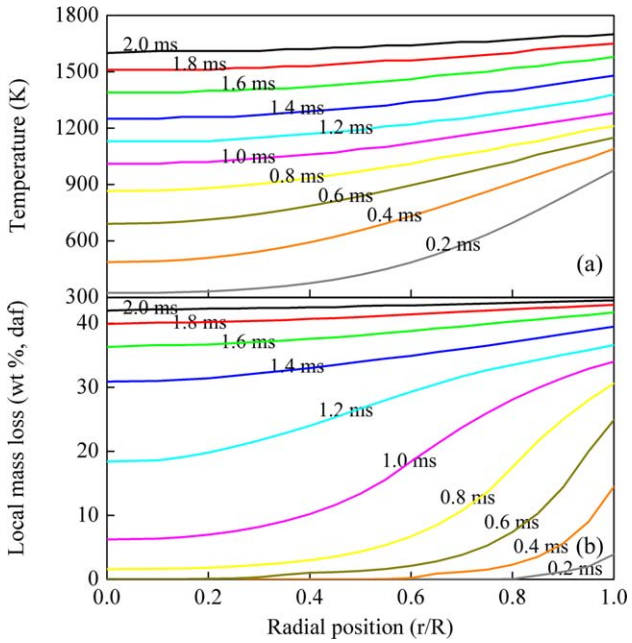

Figure 11. Predicted radial profiles of (a) temperature and (b) mass loss in at H_2 atmosphere at different time (Coal 1#, initial particle temperature 300 K, particle diameter 50 μm, surrounding temperature 1800 K).

[Color figure can be viewed in the online issue, which is available at wileyonlinelibrary.com.]

(Coal 1#) with different heats of devolatilization were investigated. The endothermic heat of devolatilization was set to 0, 420, 800, and 1350 kJ/kg, according to our experimental data and the reported results by Freihaut[37] and Hertzberg and Zlochower[38] The other computational details are the same as those of Case 4 in the last section. The variations of the average temperature and yield of volatiles of the particle with time under the atmosphere of H_2 and Ar are presented in Figure 12a, b, respectively.

It can be seen that the endothermic reaction heat of devolatilization shows significant effect on the average particle temperature history and volatiles evolution of the particle, especially during the time-interval when the volatiles are rapidly released (e.g., 0.8–2.0 ms in H_2 atmosphere and 3.0–8.0 ms in Ar atmosphere, as shown in Figure 12). The heat of devolatilization would weaken the particle heating rate and then lead to a long heating-up and devolatilization time, which is consistent with the experimental work by Liu et al.[25] The larger the heat of devolatilization, the longer the time required to completely finish the devolatilization reactions. Because the effect of the reaction heat of devolatilization on coal pyrolysis is principally determined by the devolatilization rate rather than by the intensity of heat transfer, it seems that the influence of heat of devolatilization on coal devolatilization performance is independent of the pyrolysis atmosphere. Therefore, the volatiles evolution is mainly affected by the coupling of the local temperature and apparent reaction rate.

Also the variations of the maximum temperature difference and volatiles yield difference inside particle as a function of residence time with different heats of devolatilization under the atmosphere of H_2 and Ar are plotted in Figure 13. The transient maximum temperature difference curves show that two extreme values exist when the heat of devolatilization is taken into account, no matter whether in H_2 atmosphere or in Ar atmosphere. The former extremum is primarily caused by the heat conduction while the latter extremum is mainly due to the endothermic effect of pyrolysis. The peak value of the maximum temperature difference

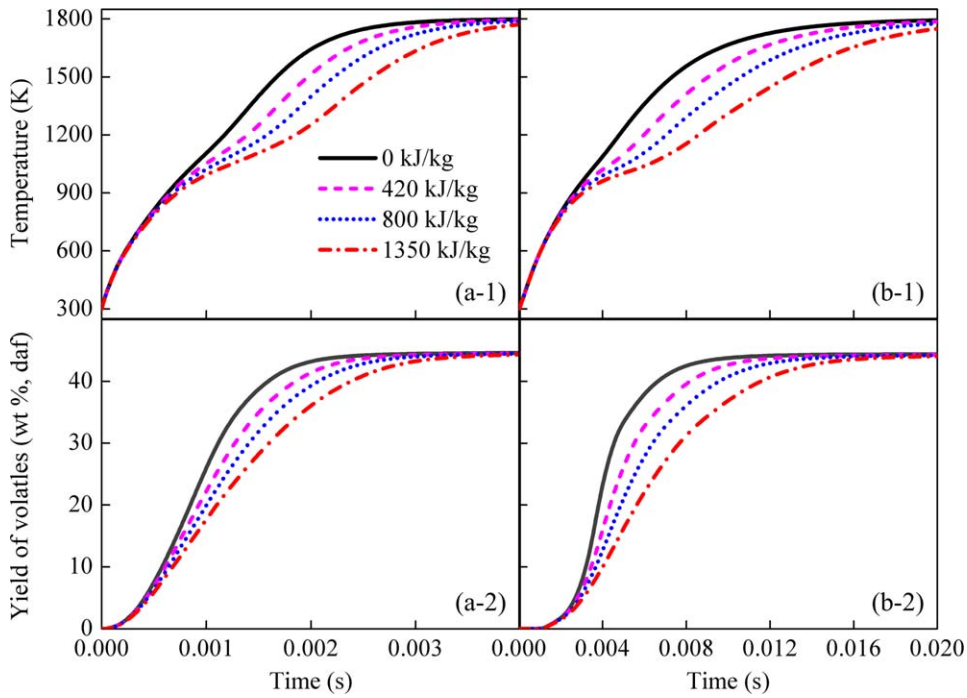

Figure 12. Variations of (1) particle average temperature and (2) yield of volatiles with time in (a) H_2 atmosphere and (b) Ar atmosphere at different heats of devolatilization (Coal 1#, initial particle temperature 300 K, particle diameter 50 μm, surrounding temperature 1800 K).

[Color figure can be viewed in the online issue, which is available at wileyonlinelibrary.com.]

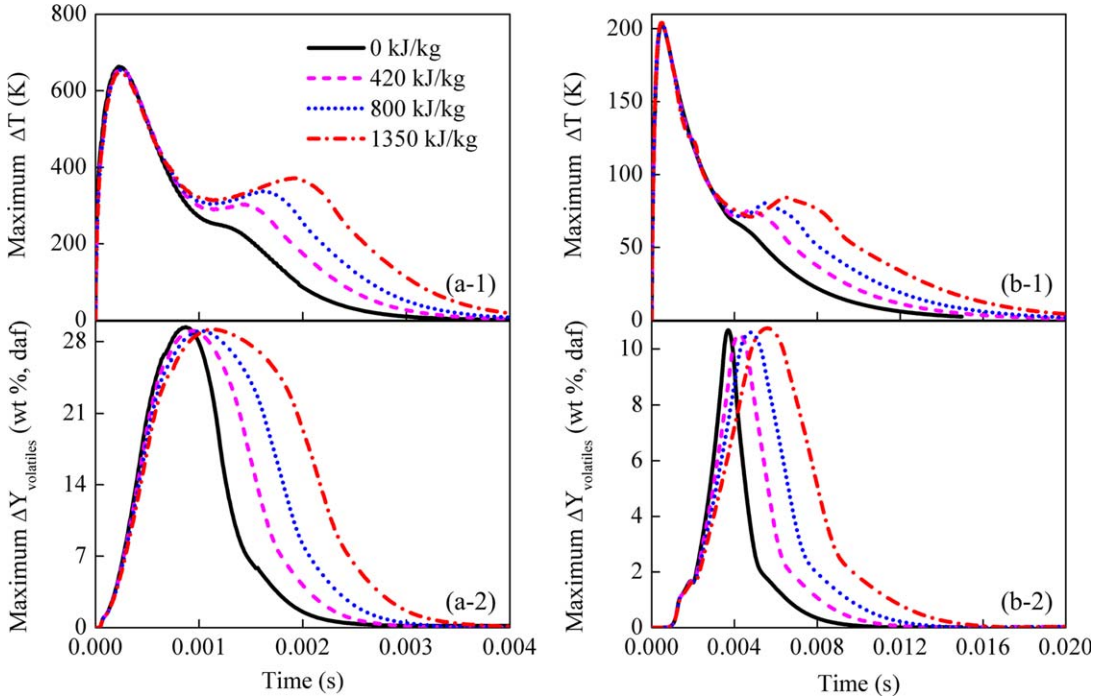

Figure 13. Variations of (1) maximum temperature difference and (2) maximum volatiles yield difference inside particle with time in (a) H2 atmosphere and (b) Ar atmosphere at different heats of devolatilization (Coal 1#, initial particle temperature 300 K, particle diameter 50 μm, surrounding temperature 1800 K).

[Color figure can be viewed in the online issue, which is available at wileyonlinelibrary.com.]

caused by the heat of devolatilization will increase with the increase of the heat of devolatilization. Therefore, it can be concluded that a precise measurement of the reaction heat of devolatilization is crucial for the accurate prediction of coal devolatilization behavior, especially when the residence time is not long enough.

It should be noted that all the simulations are based on the assumption that the effect of the single particle on the surrounding gas is ignored. The mechanism model in this article is only used to reveal the devolatilization behavior of a single particle under designed conditions and to clarify the importance of the submodels. In a practical coal conversion process, however, the component and temperature of the surrounding gas will change significantly once the devolatilization reactions occur, and then the thermodynamic and transport properties of gaseous phase consequently change, so that the coal particles would experience different pyrolysis conditions. It is expected that the model established in this article would be further used for describing the complex coal devolatilization behaviors in the practical reactor with the consideration of the interaction between the discrete particle phase and the continuum surrounding gas.

Conclusions

A comprehensive *heat transfer* and *volatiles evolution* model has been established to describe the complex *internal* heat transport and pyrolysis behavior of a single particle for various coal types under a broader range of operating conditions. The *particle-scale* physics such as the conductive heat transfer, the impeditive effect of volatiles diffusion and the endothermic effect of devolatilization reactions inside particle were taken into account in the model. The CPD model was adopted to describe the devolatilization behavior of the rapidly heated coal particle. The coal-independent kinetic parameters of the CPD model were refitted and the coal-dependent structure parameters were adjusted based on the experimental results to enable the reasonable predictions on pyrolysis behaviors of various coal types under a wide range of temperatures and heating rates.

This model was first used to explore the integrated effect of heating rate and coal type on coal devolatilization performance. The results revealed the typical effect of heating rate on the devolatilization behavior and justified the coals which would show a good devolatilization performance as heating rate rises, providing a preliminary coal rank selection method for industrial coal conversion processes. Furthermore, the influences of heat conduction, volatiles diffusion, and endothermic heat of devolatilization inside particle on particle temperature history and volatiles evolution were carried out. The results showed that the inherent heat-transfer resistances and endothermic heat of devolatilization would lead to a weakened heating-up rate and thereafter a longer heating-up and devolatilization time. The effect of the inherent resistance due to heat conduction was found to be quite significant when the intensity of heat transfer between the surrounding gas and the particle was strong. The effects of the inherent resistance due to volatiles diffusion and heat of devolatilization became more obvious during the time-interval when the release of volatiles was rapid. Therefore, the proposed submodels incorporated in this mechanism model should be considered seriously in coal conversion processes, especially under ultrahigh temperatures with milliseconds residence time.

The future work would take the interaction between the discrete particle phase and the continuum surrounding gas into account to better understand the complex coal devolatilization behaviors in a practical reactor. It is anticipated that this model would be further incorporated in the detailed

modeling of reactors for pyrolysis, gasification, and combustion of coal with different ranks and properties.

Acknowledgment

Financial supports from the National Basic Research Program of China (973 Program No. 2012CB720301), the National Natural Science Foundation of China (NSFC) under grant No. 20976091, the National Institute of Clean-and-Low-Carbon Energy (NICE) and Xinjiang Tianye (Group) Co. Ltd. are acknowledged.

Literature Cited

1. Bond RL, Ladner WR, Mcconnell GIT, Galbraith IF. Production of acetylene from coal, using a plasma jet. *Nature*. 1963;200:1313–1314.
2. Yan BH, Cheng Y, Jin Y. Cross-scale modeling and simulation of coal pyrolysis to acetylene in hydrogen plasma reactors. *AIChE J*. 2013;59:2119–2133.
3. Gavalas GR. Coal Science and Technology 4. Coal Pyrolysis. Amsterdam, Oxford, New York: Elsevier Scientific Publishing Company, 1982.
4. Badzioch S, Hawksley PG. Kinetics of thermal decomposition of pulverized coal particles. *Ind Eng Chem Process Res Dev*. 1970;9:521–528.
5. Kobayashi H, Howard JB, Sarofim AF. Coal devolatilization at high temperatures. *Symp (Int) Combust*. 1977;16:411–425.
6. Pitt GJ. The kinetics of the evolution of volatile products from coal. *Fuel*. 1962;41:267–274.
7. Anthony DB, Howard JB. Coal devolatilization and hydrogasification. *AIChE J*. 1976;22:625–656.
8. Lakshmanan CC, White N. A new distributed activation energy model using weibull distribution for the representation of complex kinetics. *Energy Fuel*. 1994;8:1158–1167.
9. Boudreau BP, Ruddick BR. On a reactive continuum representation of organic matter diagenesis. *Am J Sci*. 1991;291:507–538.
10. Ho TC, Aris R. On apparent second-order kinetics. *AIChE J*. 1987;33:1050–1051.
11. Caprariis BD, Filippis PD, Herce C, Verdone N. Double-gaussian distributed activation energy model for coal devolatilization. *Energy Fuel*. 2012;26:6153–6159.
12. Solomon PR, Hamblen DG, Carangelo RM, Serio MA, Deshpande GV. General-model of coal devolatilization. *Energy Fuel*. 1988;2:405–422.
13. Serio MA, Hamblen DG, Markham JR, Solomon PR. Kinetics of volatile product evolution in coal pyrolysis: experiment and theory. *Energy Fuel*. 1987;1:138–152.
14. Niksa S, Kerstein AR. FLASHCHAIN theory for rapid coal devolatilization kinetics. 1. Formulation. *Energy Fuel*. 1991;5:647–665.
15. Niksa S. FLASHCHAIN theory for rapid coal devolatilization kinetics. 2. Impact of operating conditions. *Energy Fuel*. 1991;5:665–673.
16. Niksa S. FLASHCHAIN theory for rapid coal devolatilization kinetics. 3. Modeling the behavior of various coals. *Energy Fuel*. 1991;5:673–683.
17. Grant DM, Pugmire RJ, Fletcher TH, Kerstein AR. Chemical-model of coal devolatilization using percolation lattice statistics. *Energy Fuel*. 1989;3:175–186.
18. Fletcher TH, Kerstein AR, Pugmire RJ, Grant DM. Chemical percolation model for devolatilization. 2. Temperature and heating rate effects on product yields. *Energy Fuel*. 1990;4:54–60.
19. Fletcher TH, Kerstein AR, Pugmire RJ, Solum MS, Grant DM. Chemical percolation model for devolatilization. 3. Direct use of C-13 NMR data to predict effects of coal type. *Energy Fuel*. 1992;6:414–431.
20. Genetti D, Fletcher TH, Pugmire RJ. Development and application of a correlation of (13)C NMR chemical structural analyses of coal based on elemental composition and volatile matter content. *Energy Fuel*. 1999;13:60–68.
21. Shuang Y, Wu CN, Yan BH, Cheng Y. Heat transfer inside particles and devolatilization for coal pyrolysis to acetylene at ultrahigh temperatures. *Energy Fuel*. 2010;24:2991–2998.
22. Fu WB, Zhang YP, Han HQ, Duan YN. A study on devolatilization of large coal particles. *Combust Flame*. 1987;70:253–266.
23. Adesanyaa BA, Pham HN. Mathematical modelling of devolatilization of large coal particles in a convective environment. *Fuel*. 1995;74:896–902.
24. Sadhukhan AK, Gupta P, Saha RK. Modeling and experimental investigations on the pyrolysis of large coal particles. *Energy Fuel*. 2011;25:5573–5583.
25. Liu XL, Wang G, Pan G, Wen Z. Numerical analysis of heat transfer and volatile evolution of coal particle. *Fuel*. 2013;106:667–673.
26. Spalding DB. Some Fundamentals of Combustion. London: Butterworths Scientific Publications, 1955.
27. Boulos MI, Fauchais P, Pfender E. Thermal Plasmas: Fundamentals and Applications, Vol. 1. New York: Plenum Press, 1994.
28. Veras CAG, Carvalho JA, Ferreira MA. The chemical percolation devolatilization model applied to the devolatilization of coal in high intensity acoustic fields. *J Braz Chem Soc*. 2002;13:358–367.
29. Fletcher TH, Pond HR, Webster J, Wooters J, Baxter LL. Prediction of tar and light gas during pyrolysis of black liquor and biomass. *Energy Fuel*. 2012;26:3381–3387.
30. Kauzmann W. Kinetic Theory of Gases. New York: W.A. Benjamin, 1966.
31. Badzioch S, Field MA, Gregory DR. Investigation of temperature variation of thermal conductivity + thermal diffusivity of coal. *Fuel*. 1964;43:267–280.
32. Merrick D. Mathematical models of the thermal decomposition of coal. 2. Specific heats and heats of reaction. *Fuel*. 1983;62:540–546.
33. Versteeg HK, Malalaserkera W. An Introduction to Computational Fluid Dynamics: The Finite Volume Method. New Jersey: Prentice Hall, 1995.
34. Xu WC, Tomita A. Effect of coal type on the flash pyrolysis of various coals. *Fuel*. 1987;66:627–631.
35. Griffin TP, Howard JB, Peters WB. An experimental and modeling study of heating rate and particle size effects in bituminous coal pyrolysis. *Energy Fuel*. 1993;7:297–305.
36. Yan BH, Cao CX, Cheng Y, Jin Y, Cheng Y. Experimental investigation on coal devolatilization at high temperatures with different heating rates. *Fuel*. 2013;117:1215–1222.
37. Freihaut JD. A numerical and experimental investigation of rapid coal pyrolysis. Ph.D. Thesis, Pennsylvania State University, State College, PA, 1980.
38. Hertzberg M, Zlochower IA. Devolatilization wave structures and temperatures for the pyrolysis of polymethylmethacrylate, ammonium perchlorate, and coal at combustion level heat fluxes. *Combust Flame*. 1991;84:15–37.

Manuscript received Jan. 5, 2014, and revision received Mar. 16, 2014.